J. Fluid Mech. (2001), *vol.* 449, *pp.* 61–84.
DOI: 10.1017/S0022112001006103 Printed in the United Kingdom

Vortex core behaviour in confined and unconfined geometries: a quasi-one-dimensional model

By D. L. DARMOFAL, R. KHAN, E. M. GREITZER AND C. S. TAN

Department of Aeronautics and Astronautics, Massachusetts Institute of Technology, Cambridge, MA 02139, USA

(Received 17 August 1999 and in revised form 21 June 2001)

Axisymmetric vortex core flows, in unconfined and confined geometries, are examined using a quasi-one-dimensional analysis. The goal is to provide a simple unified view of the topic which gives insight into the key physical features, and the overall parametric dependence, of the core area evolution due to boundary geometry or far-field pressure variation. The analysis yields conditions under which waves on vortex cores propagate only downstream (supercritical flow) or both upstream and downstream (subcritical flow), delineates the conditions for a Kelvin–Helmholtz instability arising from the difference in core and outer flow axial velocities, and illustrates the basic mechanism for suppression of this instability due to the presence of swirl. Analytic solutions are derived for steady smoothly, varying vortex cores in unconfined geometries with specified far-field pressure and in confined flows with specified bounding area variation. For unconfined vortex cores, a maximum far-field pressure rise exists above which the vortex cannot remain smoothly varying; this coincides with locally critical conditions (axial velocity equal to wave speed) in terms of wave propagation. Comparison with axisymmetric Navier–Stokes simulations and experimental results indicate that this maximum correlates with the appearance of vortex breakdown and marked core area increase in the simulations and experiments. For confined flows, the core stagnation pressure defect relative to the outer flow is found to be the dominant factor in determining conditions for large increases in core size. Comparisons with axisymmetric Navier–Stokes computations show that the analysis captures qualitatively, and in many instances, quantitatively, the evolution of vortex cores in confined geometries. Finally, a strong analogy with quasi-one-dimensional compressible flow is demonstrated by construction of continuous and discontinuous flows as a function of imposed downstream core edge pressure.

1. Introduction

Vortex cores in pressure gradients are a feature of many flows of technological interest. Well-known examples are the vortex above a low-aspect-ratio swept wing and the tip clearance vortex that occurs in turbomachinery blading. In these situations, as well as in many others, the central element is a vortex subjected to a pressure rise in the direction along its axis, with the possible consequence of large expansion of vortex core area. A direct result of this expansion on compressor or pump performance, for example, is decreased effective flow area, and hence decreased pressure rise capability.

The behaviour of vortex cores in pressure gradients is the subject of this paper.

The goal is to provide a unified model of such flows, in external (unconfined) as well as internal (confined) geometries. The spirit of the analysis is much akin to the use of one-dimensional compressible flow theory, namely to provide a simple tool for physical insight, understanding of flow regimes, parametric behaviour and structure, and useful estimates of the magnitudes of the effects of interest. Further, while the simplicity of the model places some limitations on the accuracy, comparison with experiments and computations give confidence that the model is a useful representation of many aspects of vortex core flows.

The model employs a control volume formulation similar to that of Landahl & Widnall (1971), extended to include time dependence, interaction with a flowing external stream, and the influence of bounding geometry and conforming geometry. While Landahl & Widnall only considered discontinuous jumps between two columnar vortex states, we show that in general both continuous and discontinuous solutions need to be considered and that the former are most likely in confined flows.

Similar models for unconfined vortex cores have previously been derived by Lundgren & Ashurst (1989), Marshall (1991, 1993), and Leonard (1994). Lundgren & Ashurst use a control volume formulation similar to that followed in this work. Marshall and Leonard employ (different) weighted residual techniques which have the advantage of allowing extension to more complex core velocity distributions. These previous models are more general than the present analysis (including the ability to describe non-axisymmetric disturbances), but in the limit of long-wave, axisymmetric disturbances, all the approaches reduce to essentially identical descriptions. The deliberate narrowing in scope of the present analysis arises from the desire to exhibit clearly the array of different physical effects that are associated with even the basic geometric configuration of a straight axisymmetric core (Mahesh 1996). While we thus re-iterate previous results for the behaviour of waves in unconfined situations and the existence of discontinuous solutions, new results are presented regarding: (i) the extension to steady and unsteady confined vortex cores where geometry is prescribed, (ii) the behaviour of smoothly varying core flows including numerous experimental and computational comparisons, and (iii) the analogy with quasi-one-dimensional compressible flow including solutions with 'vortex shocks' (Lundgren & Ashurst 1989; Marshall 1991, 1993; Krishnamoorthy & Marshall 1994; Marshall & Krishnamoorthy 1997).

Anticipating the results to be shown, we will demonstrate that the model appears to capture a number of important features of vortex cores in axial pressure gradients. A linearized analysis of wave propagation on the core shows, following Benjamin (1962), the distinction between supercritical states, for which all waves propagate downstream, and subcritical states, for which waves can also propagate upstream. The manner in which the global flow parameters affect the stabilizing effect of swirl (the 'stiffening effect of vortex lines', Yih 1980) on the Kelvin–Helmholtz instability associated with the axial velocity difference between core and free stream can also be seen explicitly. For steady, continuous vortex cores, a general closed-form solution is derived and used to analyse the sensitivity of core area growth to parameters such as swirl ratio, core-to-duct area ratio, axial velocity ratio, and pressure rise (for unconfined flow) or duct geometry (for confined flow). For unconfined flows it is shown that a maximum far-field pressure rise exists beyond which a steady, continuous flow cannot occur.

Comparisons with experiments and axisymmetric Navier–Stokes simulations show the model provides good quantitative estimates for core area behaviour in a varying-area duct. Also, the maximum theoretical far-field pressure rise correlates well with the appearance of vortex breakdown in the simulations and experiments. These com-

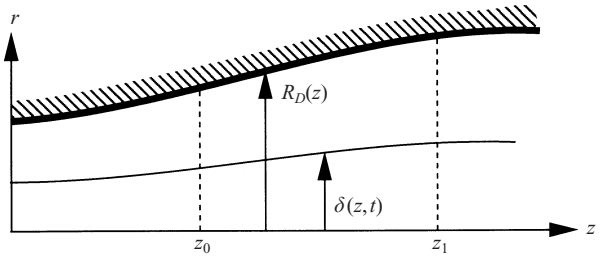

FIGURE 1. Schematic of the quasi-one-dimensional model for confined flow showing a vortex core of radius $\delta(z,t)$ with control volume end points z_0 and z_1, and pipe wall at $R_D(z)$.

parisons complement previous results of Krishnamoorthy & Marshall (1994) and Marshall & Krishnamoorthy (1997) concerning the validity of the unconfined flow model for the cutting of a vortex by a thin blade. They found that experimentally observed propagation speeds of vortex breakdowns generated by vortex cutting are consistent with the model propagation speeds of 'vortex shocks.' Marshall & Krishnamoorthy (1997) have also shown that the predictions of core area variation and force on the blade compare well with the results from direct numerical simulations.

Finally, the strong analogy with quasi-one-dimensional compressible flow is demonstrated by, to the authors' knowledge, the first construction of its kind of steady vortex core flows subjected to an external pressure gradient with an imposed downstream core pressure; the latter plays a role analogous to back pressure in quasi-one-dimensional flow. Depending on the specific conditions, there will be either smoothly varying flows or flows that include a discontinuous jump or 'vortex shock' in order to match the required back pressure. The smoothly-varying flows have a constant flux-averaged stagnation pressure throughout the domain while the discontinuous flows lose flux-averaged stagnation pressure due to the 'shock.'

2. Assumptions

The flow to be described is a Rankine (solid body rotation) vortex core, surrounded by an irrotational swirling flow. The vortex core centre is aligned with the z-axis. The core radius, δ, and axial velocity, w, are functions of axial coordinate, z, and time, t, as indicated in figure 1. At every axial location, the Rankine swirl velocity distribution is assumed, so that

$$v(r,z,t) = \begin{cases} \dfrac{\Gamma_\infty}{2\pi\delta}\dfrac{r}{\delta}, & r \leqslant \delta \\ \dfrac{\Gamma_\infty}{2\pi r}, & r > \delta, \end{cases} \tag{2.1}$$

with the far-field circulation, Γ_∞, constant. The maximum swirl velocity occurs at the core edge and is

$$v_{\max} = \frac{\Gamma_\infty}{2\pi\delta}.$$

The vortex core swirl ratio, Ω, is defined as

$$\Omega \equiv \frac{v_{\max}}{w}.$$

The fluid is taken as incompressible with constant density, ρ. In the quasi-one-dimensional treatment adopted, the core axial velocity is uniform in r.

With the approximation that the radial velocities are negligible, the radial momentum equation reduces, for steady as well as unsteady flow, to

$$\frac{\partial p}{\partial r} = \rho \frac{v^2}{r}. \tag{2.2}$$

Equations (2.1) and (2.2) plus the assumption that the flow outside the vortex core is irrotational, imply that the axial velocity outside the core is uniform in r, although its value need not be the same as in the core.

An expression for the static pressure is obtained by integrating (2.2) with the swirl velocity distribution of (2.1) to yield

$$p(r,z,t) - p_\delta(z,t) = \begin{cases} -\frac{1}{2}\rho \left(\frac{\Gamma_\infty}{2\pi\delta}\right)^2 \left[1 - \left(\frac{r}{\delta}\right)^2\right], & r \leqslant \delta \\ -\frac{1}{2}\rho \left(\frac{\Gamma_\infty}{2\pi\delta}\right)^2 \left[\left(\frac{\delta}{r}\right)^2 - 1\right], & r > \delta. \end{cases} \tag{2.3}$$

In (2.3), p_δ is the core edge pressure, $p(\delta, z, t)$.

Note that the assumptions utilized limit the applicability of this description to long-wavelength variations, in other words, situations in which axial variations occur over distances of several core radii.

3. Model equations for continuous vortex flows

Before considering specific features of confined and unconfined flows, we derive the equations that any smoothly varying (i.e. continuous) vortex core must satisfy. Consider a vortex core between axial locations z_0 and z_1 as depicted in figure 1, with differences in quantities between axial locations denoted by double brackets, i.e.

$$[[f(z)]] = f(z_1) - f(z_0).$$

Conservation of mass in the vortex core gives

$$\frac{\mathrm{d}}{\mathrm{d}t} \int_{z_0}^{z_1} A \, \mathrm{d}z + [[Aw]] = 0, \tag{3.1}$$

where the core area is $A = \pi\delta^2$. Conservation of axial momentum in the vortex core is

$$\frac{\mathrm{d}}{\mathrm{d}t} \int_{z_0}^{z_1} Aw \, \mathrm{d}z + [[Aw^2]] = -\frac{1}{\rho} \int_{z_o}^{z_1} A \frac{\partial p_\delta}{\partial z} \, \mathrm{d}z. \tag{3.2}$$

Equations (3.1) and (3.2) can also be written in differential form,

$$\frac{\partial}{\partial t}(A) + \frac{\partial}{\partial z}(Aw) = 0, \tag{3.3}$$

$$\frac{\partial}{\partial t}(Aw) + \frac{\partial}{\partial z}(Aw^2) = -\frac{A}{\rho}\frac{\partial p_\delta}{\partial z}. \tag{3.4}$$

Equations (3.3) and (3.4) (or (3.1) and (3.2)) are two equations for three unknowns, A, w and p_δ. To close the problem, the variation in edge pressure must be specified either through imposition of the far-field pressure (in the case of an unconfined flow) or the confining geometry.

For the former we use the relation between core edge and far-field pressure from (2.3),

$$p_\delta(z,t) = p_\infty(z,t) - \rho\frac{\Gamma_\infty^2}{8\pi A}. \tag{3.5}$$

Introducing (3.5), equation (3.4) becomes

$$\frac{\partial}{\partial t}(Aw) + \frac{\partial}{\partial z}\left(Aw^2 + \frac{\Gamma_\infty^2}{8\pi}\log A\right) = -\frac{A}{\rho}\frac{\partial p_\infty}{\partial z}. \tag{3.6}$$

These equations have been previously derived by Marshall (1991).

For flows in confined geometries (ducts), we define the duct in terms of a specified radius, $R_D(z)$, as depicted in figure 1, with a core flow from $0 < r < \delta(z,t)$ and an outer flow from $\delta(z,t) < r < R_D(z)$. Descriptions of conservation of mass and momentum in the outer region close the problem.

For the outer flow, conservation of mass in differential form is

$$\frac{\partial}{\partial t}(A_D - A) + \frac{\partial}{\partial z}[(A_D - A)W] = 0, \tag{3.7}$$

where $A_D = \pi R_D^2$ is the duct area and W is the axial velocity in the outer flow. In terms of the core edge pressure, p_δ, conservation of momentum in the outer region is written

$$\frac{\partial}{\partial t}[(A_D - A)W] + \frac{\partial}{\partial z}[(A_D - A)W^2] = -\frac{A_D - A}{\rho}\frac{\partial p_\delta}{\partial z} + \frac{\Gamma_\infty^2}{8\pi A}\left(\frac{A_D}{A} - 1\right)\frac{\partial A}{\partial z}. \tag{3.8}$$

Equations (3.3), (3.4), (3.7) and (3.8) describe the evolution of A, w, W and p_δ for smoothly varying confined vortex cores.

4. Waves on vortex cores and flow regime definition

To illustrate the role of wave propagation speeds as a means of differentiating behaviour regimes, and to demonstrate the stabilizing effect of swirl, we examine wave propagation along a vortex core. We linearize (3.3), (3.4), (3.7) and (3.8) by taking all quantities to be composed of a mean state, uniform in z, plus a small perturbation. The resulting equations for confined flow are

$$\frac{\partial A'}{\partial t} + w\frac{\partial A'}{\partial z} = -A\frac{\partial w'}{\partial z}, \tag{4.1}$$

$$\frac{\partial w'}{\partial t} + w\frac{\partial w'}{\partial z} = -\frac{1}{\rho}\frac{\partial p'_\delta}{\partial z}, \tag{4.2}$$

$$\frac{\partial A'}{\partial t} + W\frac{\partial A'}{\partial z} = (A_D - A)\frac{\partial W'}{\partial z}, \tag{4.3}$$

$$\frac{\partial W'}{\partial t} + W\frac{\partial W'}{\partial z} = -\frac{1}{\rho}\frac{\partial p'_\delta}{\partial z} + \frac{\Gamma_\infty^2}{8\pi A^2}\frac{\partial A'}{\partial z}, \tag{4.4}$$

where primed variables denote the small perturbations and unprimed here refer to the mean flow. Equations (4.1)–(4.4) are a long-wavelength description of wave propagation on the vortex core. Decomposing the perturbations into individual Fourier modes such that $A'(z,t) = \hat{A}\exp \mathrm{i}(kz - \omega t)$, where k and ω are the disturbance wavenumber and frequency, respectively, and substituting into the linear equations, (4.1)–(4.4) lead to an eigenvalue problem for the wave speed $\lambda = \omega/k$.

4.1. *Unconfined flows*

For the unconfined case (the limit of infinite duct radius), the eigenvalues are

$$\lambda_{1,2} = w \pm c, \tag{4.5}$$

where the quantity, c, is defined

$$c^2 \equiv \frac{\Gamma_\infty^2}{8\pi A} = \frac{v_{\max}^2}{2}. \tag{4.6}$$

Flow disturbances travel at characteristic speeds, $w \pm c$, and two regimes can thus be defined (Benjamin 1962). For $|w| - c > 0$, referred to as supercritical, all disturbances move downstream. For $|w| - c < 0$, referred to as subcritical, disturbances can propagate both up- and downstream. Analogous to the Mach number, we define a dimensionless number, $\mathscr{R}$, using the axial velocity and the small disturbance speed to characterize the vortex state. When $|\mathscr{R}| > 1$ the flow is supercritical and when $|\mathscr{R}| < 1$ the flow is subcritical. Specifically,

$$\mathscr{R} = \frac{w}{c} = \frac{\sqrt{2}}{\Omega},$$

where Ω is the swirl number $v_{\max}/w$. $\mathscr{R}$ can be regarded as a Rossby number based on core angular velocity and radius. The condition $\mathscr{R} = 1$ has been previously used as a criterion for classifying vortices and impending vortex breakdown by Spall, Gatski & Grosch (1987). At this condition the swirl ratio is $\Omega_{\text{crit}} = \sqrt{2}$, and a vortex is supercritical when the swirl ratio, $\Omega < \Omega_{\text{crit}}$.

Some indication of the effect of the model approximations can be seen by comparing the critical swirl ratio ($\Omega_{\text{crit}} = \sqrt{2}$) given above with that resulting from eigensolutions of the inviscid small disturbance equations (Benjamin 1962; Marshall 1993) for a Rankine vortex, which yield a critical swirl ratio of approximately 1.2. As will be seen for other aspects, the quasi-one-dimensional model not only provides a useful estimate of this and other 'exact' numerical values, but is in good accord with qualitative trends seen in more complex descriptions and experiments.

4.2. *Confined flows*

For confined vortex flow, the eigenvalues are

$$\lambda_{1,2} = \frac{(A_D - A)w + A\,W}{A_D} \pm \sqrt{\left(1 - \frac{A}{A_D}\right)\left[c^2 - \frac{A}{A_D}(W - w)^2\right]}. \tag{4.7}$$

In (4.7), c is the vortex core wave speed defined in (4.6). If we define effective convective and wave speeds as

$$w_{\text{eff}} = w\left[1 + \frac{A}{A_D}\left(\frac{W}{w} - 1\right)\right],$$

$$c_{\text{eff}}^2 = \left(1 - \frac{A}{A_D}\right)\left[c^2 - \frac{A}{A_D}(W - w)^2\right],$$

the eigenvalues can be written as $\lambda_{1,2} = w_{\text{eff}} \pm c_{\text{eff}}$.

For the confined case the eigenvalues can be complex, corresponding to the long-wavelength Kelvin–Helmholtz instability of the cylindrical vortex sheet separating core and outer flow. For purely real eigenvalues c_{eff}^2 must be equal to or greater than

zero, or

$$\frac{\Gamma_\infty^2}{8\pi A} \geqslant \frac{A}{A_D}(W-w)^2. \tag{4.8}$$

Equation (4.8) shows the stabilizing effect of swirl: the larger the difference in axial velocity between core and outer region, the greater the swirl needed for stability. The analogy between the stability of axisymmetric rotating fluids and stratified fluid motion in a gravitational field (e.g. Howard 1963; Drazin & Reid 1981) can be seen directly by comparison of (4.7) with the corresponding equation for long waves in two-layer stratified flow (e.g. Lamb 1932). In that case, the stabilization arises from the difference in density of the fluids. We note that (4.8) offers no information about, and indeed cannot be applied to, stability of the unbounded vortex core. The long-wavelength approximation is based on the disturbance wavelength being much larger than any characteristic geometric length scale in the problem (for example the duct radius, R_D). The one-dimensional description of Kelvin–Helmholtz instability which results from this approximation, and which implies that the perturbations are independent of radial position, cannot be used for an unbounded flow. To analyse stability, the long-wavelength description can be used in the core, but it would need to be coupled with a two-dimensional (z, r) description of the motion in the unbounded irrotational flow outside the core which allows pressure and velocity perturbations in the external flow to decay appropriately with distance away from the core.

For the confined case, an effective criticality parameter can be defined as

$$\mathscr{R}_{\text{eff}} = \frac{w_{\text{eff}}}{c_{\text{eff}}},$$

with values of $\mathscr{R}_{\text{eff}} > 1$ indicating supercritical flow. For given A/A_D and w/W, the critical swirl ratio for which $\mathscr{R}_{\text{eff}} = 1$ is

$$\Omega_{\text{crit}} = \sqrt{2\left[1 + \frac{(W/w)^2}{A_D/A - 1}\right]}. \tag{4.9}$$

These critical values mark the boundary between subcritical and supercritical flows. They will be seen to indicate the condition under which core area growth becomes locally unbounded and hence to mark parameter regimes with rapid core expansion.

5. Vortex core growth in steady continuous flow

Two issues are addressed in this section. The first is development of criteria for conditions under which large growth in vortex core area is expected. From a technological perspective, this is perhaps the most important problem associated with vortex core flows. In this, the (non-dimensional) flux-averaged core stagnation pressure will be shown to have a central role. The second is to assess, through comparison with experiments and with axisymmetric time-accurate Navier–Stokes simulations, the degree to which the present model provides a useful description for the flows of interest.

To examine the flux-averaged core stagnation pressure, (3.3) and (3.4) can be combined to give

$$\frac{\partial}{\partial z}(p_\delta + \tfrac{1}{2}\rho w^2) = 0. \tag{5.1}$$

The quantity $p_\delta + \frac{1}{2}\rho w^2$ is the core flux-averaged stagnation pressure which will be

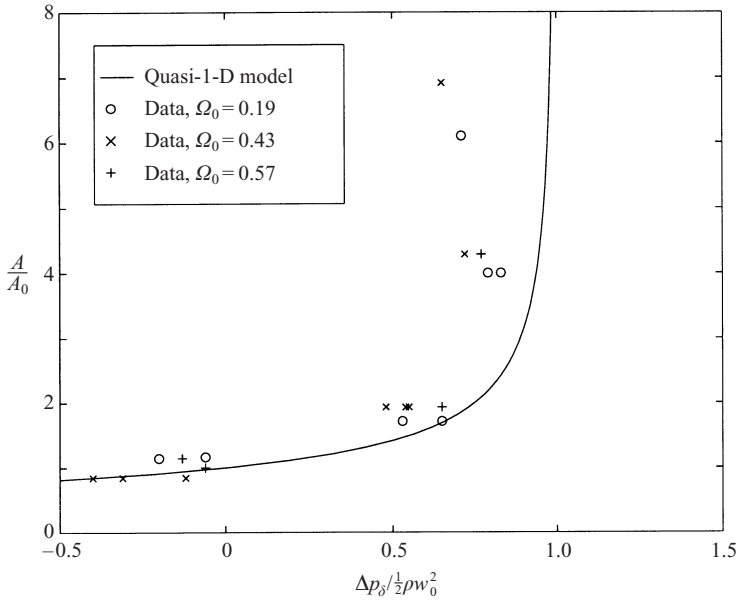

FIGURE 2. Vortex core expansion A/A_0 versus edge pressure rise $\Delta p_\delta / \frac{1}{2}\rho w_0^2$ for inlet swirl $\Omega_0 = 0.19$, 0.43 and 0.57. Data by Cho (1995). The upstream core-to-duct area ratio $A_0/A_{D_0} \approx 0.04$ and the pressure rise occurred over an axial distance of approximately 40 core radii.

denoted by, $\bar{H}_{\text{core}}$; it is defined as

$$\bar{H}_{\text{core}} \equiv \frac{2\pi}{Aw}\int_0^\delta [p + \tfrac{1}{2}\rho(v^2 + w^2)]wrdr = p_\delta + \tfrac{1}{2}\rho w^2, \tag{5.2}$$

where (2.1) and (2.3) have been used. Equations (5.1) and (5.2) show that under the assumptions made here $\bar{H}_{\text{core}}$ is constant for a steady continuous vortex.

Equation (5.1) can be regarded as a quasi-Bernoulli relation between core edge pressure and core velocity. Invoking continuity this can be written in a form that connects changes in core area and core edge static pressure,

$$\frac{\Delta p_\delta}{\frac{1}{2}\rho w_0^2} = 1 - \left(\frac{A_0}{A}\right)^2, \tag{5.3}$$

where A_0 and w_0 are the initial core area and axial velocity, and Δp_δ is the pressure rise from the initial to current location. Equation (5.3) has been derived without considerations of the outer flow and applies to both confined and unconfined geometries and all values of swirl.

The validity of (5.1) and thus of the overall core model has been examined experimentally by Cho (1995). The experiments consisted of a constant-area duct, with the pressure rise created by flow extraction at the outer wall. In the experiments, the upstream core-to-duct area ratio $A_0/A_{D_0} \approx 0.04$ and the pressure rise occurred over an axial distance of approximately 40 core radii. Additional information about the experiment can be found in Cho (1995).

Figure 2 shows core area variation as a function of core edge pressure rise, $\Delta p_\delta = p_\delta - p_{\delta 0}$ where $p_{\delta 0}$ is the upstream edge pressure. For lower pressure rises, the experimental and quasi-one-dimensional results compare well. At the higher pressure rises, the core area increases are several times greater than those encountered in

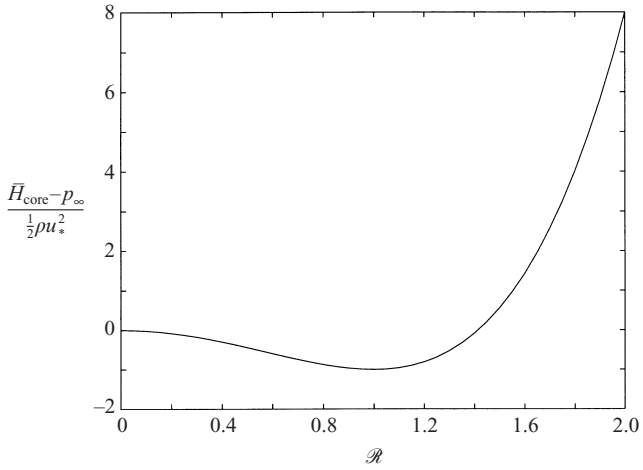

FIGURE 3. Variation with $\mathscr{R}$ of the relationship of stagnation pressure, $\bar{H}_{\text{core}}$, and far-field pressure, p_∞, for a steady flow.

numerical simulations at the onset of vortex breakdown. These latter conditions are perhaps outside the ability of the theory to describe because the large radial expansions and associated large radial velocities are not modelled. Figure 2 however, does show the applicability of the description summarized by (5.3) and also indicates that the theory provides a quantitative estimate of the conditions (i.e. value of Δp_δ) when rapid growth will occur.

5.1. *Unconfined flows*

For an unconfined vortex, the effect of external conditions is expressed by the far-field pressure distribution, $p_\infty(z)$. The far-field pressure can be related to the core stagnation pressure and the criticality parameter, $\mathscr{R}$, by

$$\frac{\bar{H}_{\text{core}} - p_\infty}{\frac{1}{2}\rho u_*^2} = \mathscr{R}^2\left(\mathscr{R}^2 - 2\right), \tag{5.4}$$

where u_* is a reference velocity given by

$$u_* = \frac{\Gamma_\infty^2}{8\pi A w}.$$

For a steady flow, u_* and $\bar{H}_{\text{core}}$ are invariants. Equation (5.4) provides a relation between the far-field pressure and the criticality parameter $\mathscr{R}$ which is illustrated in figure 3. Increases in far-field pressure always drive $\mathscr{R}$ towards unity regardless of the value of $\mathscr{R}$. The difference between the flux-averaged core stagnation pressure and the far-field pressure reaches a minimum when $\mathscr{R} = 1$, given by

$$\min_{\text{all }\mathscr{R}}(\bar{H}_{\text{core}} - p_\infty) \equiv \bar{H}_{\text{core}} - p_\infty^* = \left(\bar{H}_{\text{core}} - p_\infty\right)\big|_{\mathscr{R}=1} = -\tfrac{1}{2}\rho u_*^2.$$

If the far-field pressure is greater than p_∞^*, the core cannot remain smoothly varying and a dissipative discontinuity (analogous to a shock in compressible flow) develops and propagates upstream. For these situations the stagnation pressure drops across the discontinuity (see § 6), decreasing $\bar{H}_{\text{core}} - p_\infty^*$ further, leading to the conclusion that steady flows with static pressure above p_∞^* do not exist whether or not the flow is continuous.

Another feature associated with critical conditions ($\mathscr{R} = 1$ or equivalently $\Omega = \sqrt{2}$ for unconfined flows) is that the local rate of change of core area, as a function of p_∞, becomes unbounded. This can be seen by combining the steady form of (3.3), (3.4) and (3.5) to yield

$$\frac{\mathrm{d}A}{A} = \frac{1}{1 - \Omega^2/2} \frac{\mathrm{d}p_\infty}{\rho w^2} = \frac{\mathscr{R}^2}{\mathscr{R}^2 - 1} \frac{\mathrm{d}p_\infty}{\rho w^2}. \tag{5.5}$$

Equation (5.5) provides an argument for the connection between critical conditions and the onset of rapid core growth, which we amplify in the following sections.

5.1.1. *Model comparison with numerical and experimental results*

To investigate the existence of a maximum pressure rise for smoothly varying flows, numerical simulations of the incompressible, axisymmetric Navier–Stokes equations have been performed utilizing the time-accurate, streamfunction–vorticity algorithm developed by Darmofal (1993, 1996). This algorithm has been validated by comparisons with experimental data for a variety of swirling flows including vortex breakdown by Darmofal (1996). The results below show that the maximum pressure rise given by the core model corresponds closely with the pressure rise at the onset of vortex breakdown in the numerical simulations. This connection between vortex breakdown and the existence of a maximum pressure rise at critical conditions also relates to the numerical results of Darmofal & Murman (1994) for axisymmetric viscous flows where it was found that vortex breakdown would occur when an upstream supercritical vortex became locally critical.

In the computations a far-field pressure distribution was imposed of the form

$$C_{p_\infty} = C_{p_{\infty\max}} \exp\left[-\left(\frac{z - z_{\max}}{\Delta z} \right)^2 \right], \tag{5.6}$$

where

$$C_{p_\infty} \equiv \frac{p_\infty - p_{\infty a}}{\frac{1}{2}\rho u_*^2}, \tag{5.7}$$

and $p_{\infty a}$ is the upstream far-field pressure. In (5.6), $C_{p_{\infty\max}}$, $z_{\max}$, and Δz are input parameters representing the maximum pressure coefficient, the location of maximum pressure, and the spatial extent of the pressure rise, respectively. The important feature is the existence of a local maximum in static pressure rather than the precise shape; other distributions have been examined with similar results.

The computational procedure was to obtain a steady solution without vortex breakdown by marching time accurately to steady state for low $C_{p_{\infty\max}}$. Then, using this steady solution as an initial condition, $C_{p_{\infty\max}}$ was raised and the flow evolved in time until either it became steady or vortex breakdown, identified by the occurrence of reversed flow, appeared in the transient Navier–Stokes simulations. In the case of a steady flow, $C_{p_{\infty\max}}$ was raised and the flow evolved again. The value of $C_{p_{\infty\max}}$ at which vortex breakdown first occurred was then compared to the maximum pressure rise given by the model, $C^*_{p_\infty}$,

$$C^*_{p_\infty} = 1 + \mathscr{R}_a^2(\mathscr{R}_a^2 - 2),$$

where $\mathscr{R}_a$ is the upstream Rossby number of the vortex core. The maximum pressure rise can also be written in terms of the upstream stagnation pressure in the core. Specifically,

$$C^*_{p_\infty} = 1 + C_{Ha},$$

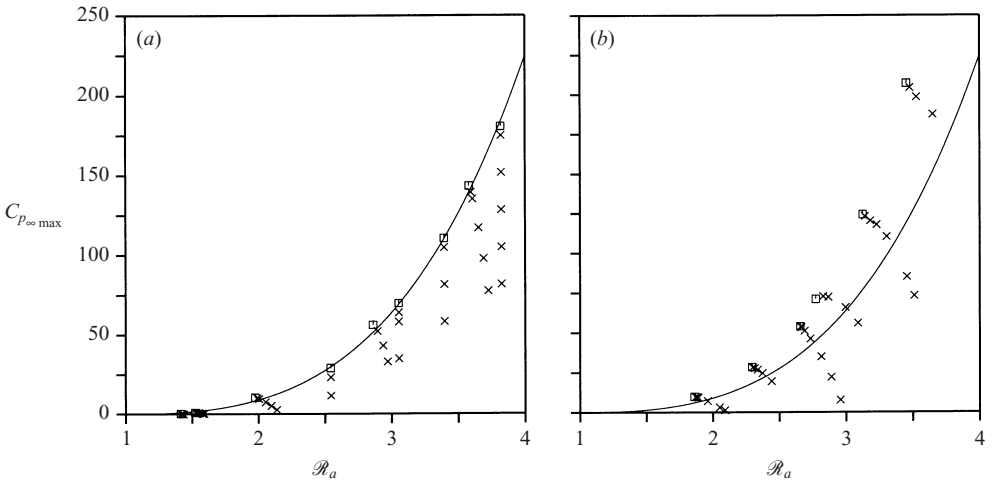

FIGURE 4. Comparison of maximum pressure rise for smoothly varying flows from model, $C^*_{p_\infty}$, with Navier–Stokes (N–S) prediction of pressure rise at breakdown onset. □, N–S solutions with breakdown; ×, N–S solutions without breakdown; solid line, model prediction for $C^*_{p_\infty}$. (*a*) Rankine vortex inlet condition. (*b*) q-vortex inlet condition.

where C_{Ha} is the upstream value of the stagnation pressure coefficient defined by

$$C_H \equiv \frac{\bar{H}_{\text{core}} - p_{\infty a}}{\frac{1}{2}\rho u_*^2}. \tag{5.8}$$

Computations were carried out based on two different inlet conditions: a Rankine vortex, which corresponded to the approximation in the model, and a more realistic, 'q-vortex' profile, which matches a number of experimentally measured profiles (Faler & Leibovich 1977). Comparisons with the latter thus give an estimate of the ability of the quasi-one-dimensional model to describe actual vortex flows. The form of the q-vortex(Batchelor 1964; Leibovich 1983) is

$$\begin{aligned} u_0(r) &= 0, \\ \Gamma_0(r) &= \Omega\left[1 - \exp(-r^2)\right], \\ w_0(r) &= 1 + \Delta w \exp(-r^2). \end{aligned}$$

Here, r is the radial coordinate (made non-dimensional by dividing by the core radius) and Δw is the difference between the axial velocity at the axis and in the far-field, made non-dimensional by dividing by far-field velocity. For a q-vortex the radial location for maximum swirl is approximately $r_{\max} = 1.1$. All computations were run at Reynolds number of 1000 based on upstream core radius and far-field velocity because previous numerical results showed the influence of viscous effects is minimal for $Re > 500$ (Darmofal 1993).

Figure 4 compares the maximum pressure rise from the model with breakdown onset from the Navier–Stokes computations for Rankine and q-vortex profiles. The length of the numerical domain was 40 core radii and the far-field pressure Δz and $z_{\max}$ are 40 and 20 respectively. Numerical solutions without breakdown are indicated by × symbols with the open square indicating the value of $C^*_{p_\infty}$ for which breakdown occurred. Agreement between the one-dimensional model and the Navier–Stokes solutions for Rankine inlet profiles is very good. For the q-inlet profile, the

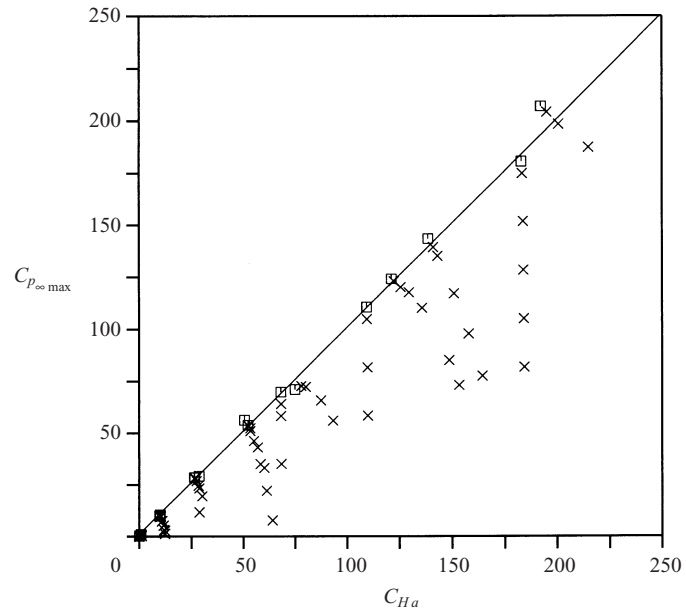

FIGURE 5. All inlet conditions. Correlation with C_{Ha}. Comparison of model prediction versus Navier–Stokes prediction of breakdown onset. □, N–S solutions with breakdown; ×, N–S solutions without breakdown; solid line, model prediction for $C^*_{p\infty}$.

qualitative trends are captured, although there is a quantitative difference in onset points.

Plotting the results in the form of $C^*_{p\infty}$ versus the inlet flux-averaged stagnation pressure coefficient, C_{Ha}, allows all the computational results to be collapsed to essentially a single bounding curve, as shown in figure 5. The one-dimensional approach based on the value of flux-averaged stagnation pressure gives a useful quantitative estimate of the conditions at which vortex breakdown occurs. Although we have found the flux-averaged stagnation pressure coefficient to effectively correlate results for Rankine (i.e. plug flow) and non-Rankine vortices, Krishnamoorthy & Marshall have also successfully employed a different approach defining an effective core radius by matching the axial velocity profile to a Gaussian distribution (Krishnamoorthy & Marshall 1994; Marshall & Krishnamoorthy 1997). We have not pursued this possibility.

Experiments reported by Pagan (1989) can also be used to assess the utility of the maximum pressure rise given by the model. The experiments used a vortex generator made of two airfoils set at opposite angles of incidence, with the resulting vortex subjected to varying pressure gradients. A flow regime map of swirl ratio versus pressure rise was obtained on which a limiting curve defined a region above which breakdown, i.e. rapid core expansion, occurred. The experimental results are plotted in figure 6, along with the curve showing the locus of critical behaviour given by the analysis. The quasi-one-dimensional analysis has trends similar to the data with the maximum pressure rise increasing as the swirl decreases, although breakdown occurs in the experiments at a swirl ratio approximately 25% lower than the model. We can connect this to the comments made in § 4.1 comparing the present model with the exact analysis. If breakdown can be associated with local criticality, the comparison in § 4.1 would imply that the simple theory, which predicts a higher

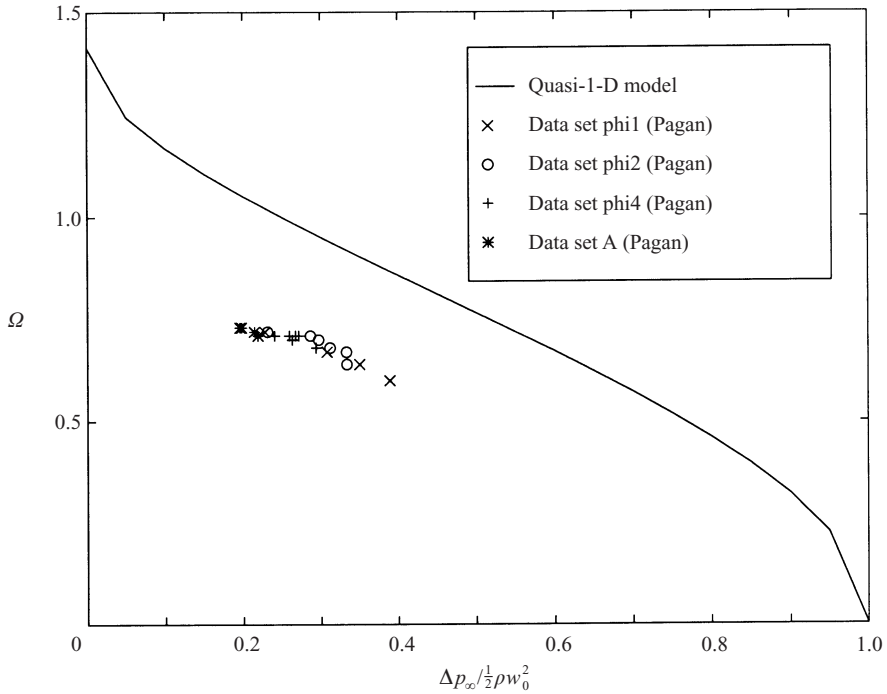

FIGURE 6. Swirl ratio Ω versus pressure rise $\Delta p_\infty / \frac{1}{2}\rho w_0^2$ showing limiting curve for vortex breakdown for an unconfined vortex. Data by Pagan (1989).

value of swirl for critical conditions, would be above the experiments by roughly 17%.

5.1.2. *Parametric trends for core area behaviour*

A useful attribute of the model is analysis of parametric trends. To describe these, it is helpful to expand the quasi-Bernoulli equation, (5.1), into an expression that explicitly displays parameters such as initial swirl level and far-field pressure rise, which could be specified in a given experiment. Using (5.4) with the constancy of core mass flow and $\bar{H}_{\text{core}}$, the desired relationship is

$$\frac{\Omega_0^2}{A/A_0} - \left(\frac{1}{A/A_0}\right)^2 - \frac{\Delta p_\infty}{\frac{1}{2}\rho w_0^2} = \Omega_0^2 - 1, \tag{5.9}$$

where $\Delta p_\infty = p_\infty - p_{\infty 0}$ and Ω_0 is the swirl ratio at upstream conditions.

Variation of A/A_0 with far-field pressure change is plotted in figure 7 for upstream swirl ratios in the range $0 \leqslant \Omega_0 \leqslant 2.5$ in increments of 0.5. Several features can be seen. First, the variation of core area with respect to far-field pressure changes sign when the flow switches from subcritical to supercritical conditions. For supercritical vortices, increases in far-field pressure create decreases in the core axial velocity and increases in core area. Thus, $\mathrm{d}A/\mathrm{d}p_\infty > 0$, qualitatively similar to behaviour in non-swirling flows. Conversely, decreases in far-field pressure produce decreases in core area. For subcritical vortices (strong swirl), the situation is reversed: increases in far-field pressure are associated with accelerations of the core and decreases in core area, with $\mathrm{d}A/\mathrm{d}p_\infty < 0$. The trend between changes in p_δ and area, however,

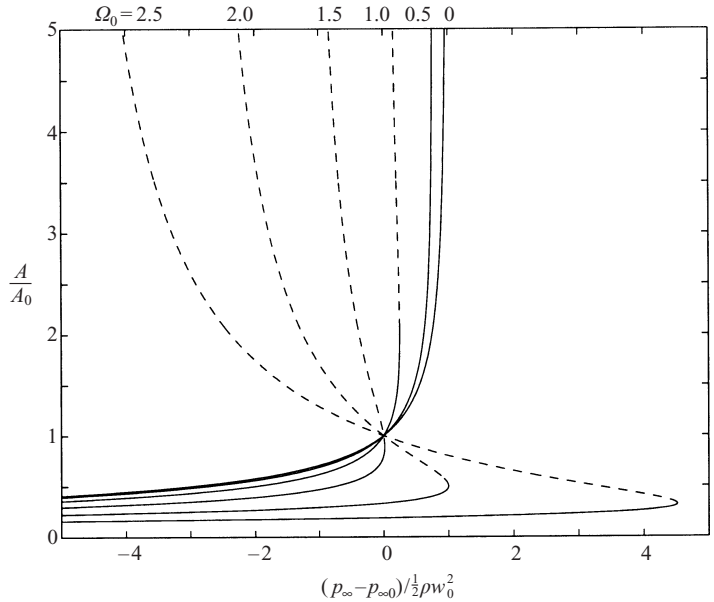

FIGURE 7. Dependence of A/A_0 on the far-field pressure for flows with $\Omega_0 = 0$, 0.5, 1.0, 1.5, 2.0 and 2.5. The solid lines are supercritical flows and the dashed lines are subcritical flows.

is independent of flow regime, so the relationship between changes in p_δ and p_∞ switches sign at critical conditions.

Another aspect seen in figure 7 is the existence of a maximum pressure rise for each value of inlet swirl, Ω_0 which, as described previously, coincides with the vortex becoming locally critical (local swirl ratio of $\sqrt{2}$). At this condition, the local rate of increase of area as a function of far-field pressure is unbounded and the core area A/A_0 is $2/\Omega_0^2$. The maximum pressure rise is therefore a function of the inlet swirl only, given by

$$\frac{\Delta p_\infty^*}{\frac{1}{2}\rho w_0^2} = 1 - \Omega_0^2 + \frac{\Omega_0^4}{4}.$$

5.2. *Confined flows*

For steady, smoothly varying, confined vortex flows, the outer flow is irrotational with uniform stagnation pressure. In examining the behaviour of a confined flow, the quantities specified are typically the duct area schedule and three non-dimensional parameters characterizing the inlet state. One choice of the three parameters is inlet axial velocity ratio $\alpha_0 = W_0/w_0$, inlet area ratio $\sigma_0 = A_0/A_{D_0}$ and inlet swirl ratio $\Omega_0 = v_{\max 0}/w_0$. In terms of these parameters application of the constancy of mass flow and $\bar{H}$ in both core and outer flows leads to an equation for core area,

$$\frac{\Omega_0^2}{A/A_0} - \left(\frac{1}{A/A_0}\right)^2 + \left[\frac{\alpha_0(1-\sigma_0)}{A_D/A_{D_0} - \sigma_0 A/A_0}\right]^2 = \Omega_0^2 - 1 + \alpha_0^2. \tag{5.10}$$

The change in core area due to changes in duct area is found by differentiating (5.10),

$$\frac{\mathrm{d}A}{A} = 2\frac{(W/w)^2}{(\Omega_{\mathrm{crit}}^2 - \Omega^2)(1 - A/A_D)}\frac{\mathrm{d}A_D}{A_D}, \tag{5.11}$$

where Ω_{crit} is the critical swirl ratio for confined flows defined in (4.9). Equation (5.11) shows that core area variations with respect to duct area variations become

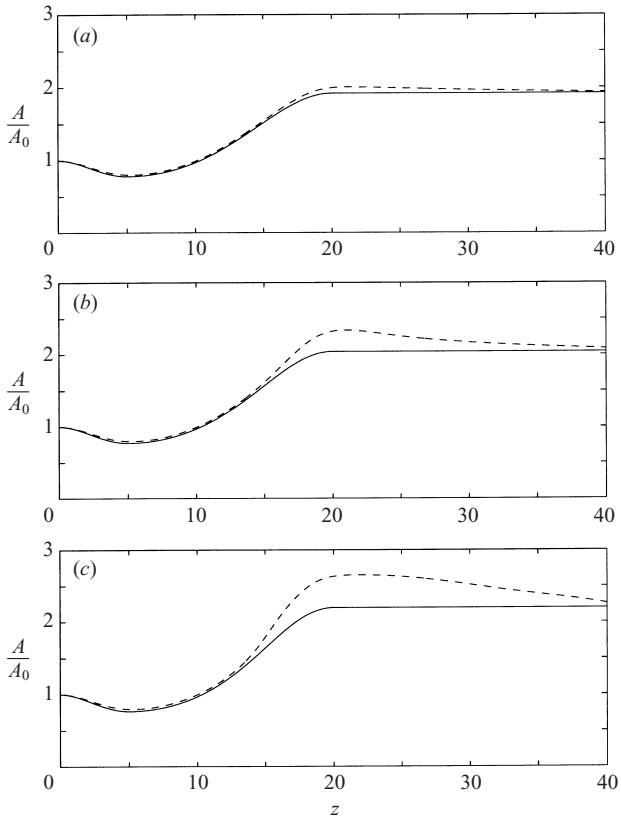

FIGURE 8. Core area variation for confined vortex flow in a converging–diverging pipe for $\alpha_0 = 0.92$ (wake) and $\sigma_0 = 0.3025$. Quasi-one-dimensional A/A_0: solid line; Navier–Stokes with q-vortex inlet condition A/A_0: dashed line. (*a*) $\Omega_0 = 0.56$, (*b*) 0.67, (*c*) 0.78.

unbounded when the local swirl ratio is critical, analogous to the behaviour of unconfined vortex cores. The critical swirl condition thus plays a dominant role in the growth of vortex cores for both unconfined and confined flows.

5.2.1. *Model comparison with numerical simulation*

To assess the quasi-one-dimensional flow field description in a more detailed fashion, we again utilize the axisymmetric Navier–Stokes algorithm of Darmofal (1993). The main goal is to determine how well the evolution of integral core properties is captured by the model. For the Navier–Stokes results, the core radius at a given axial location is defined by the stream surface that encloses the inlet core mass flux, with the inlet core radius taken at the location of maximum swirl.

A converging–diverging duct geometry is used similar to that of Beran & Culick (1992). The solver models the wall flow as an inviscid slip boundary so that the focus can be on vortex core behaviour rather than wall boundary layer effects. The specific duct geometry used is given by

$$R(z) = \begin{cases} R_i + \frac{1}{2}(R_t - R_i)\{1 - \cos[\pi(z/z_t)]\}, & 0 \leqslant z \leqslant z_t \\ R_t + \frac{1}{2}(R_o - R_t)\{1 - \cos[\pi(z - z_t)/(z_o - z_t)]\}, & z_t \leqslant z \leqslant z_o \\ R_o, & z_o \leqslant z \leqslant z_{\max}. \end{cases}$$

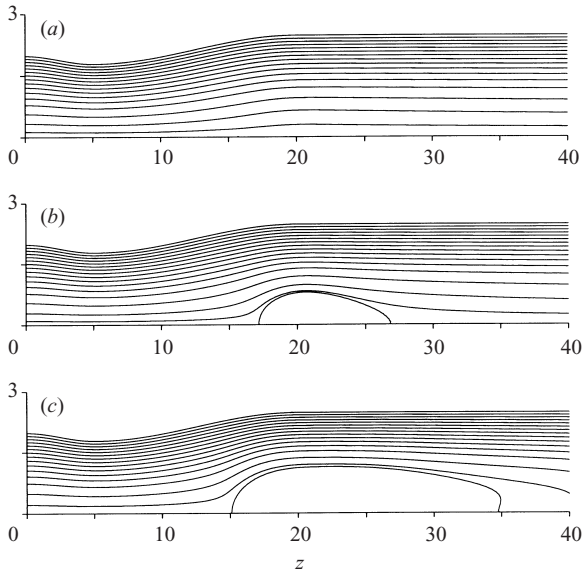

FIGURE 9. Contour plots of streamsurfaces from the Navier–Stokes solver for confined vortex flow in a converging–diverging pipe with $\alpha_0 = 1.09$ (wake) and $\sigma_0 = 0.3025$. (*a*) $\Omega_0 = 0.56$, (*b*) 0.67, (*c*) 0.78.

In the simulations, inlet velocity and area ratios were held constant at $\alpha_0 = 1.09$ (i.e. a slight wake) and $\sigma_0 = 0.3025$, respectively. The duct geometry parameters were $z_t = 5$, $z_o = 20$, $z_{\max} = 40$, $R_i = 2$, $R_t = 1.8$, and $R_o = 2.5$, all non-dimensionalized by inlet core radius. Comparisons of the quasi-one-dimensional model and Navier–Stokes simulations are shown in figure 8 for three values of Ω_0 covering situations without breakdown and with breakdown and recirculation. Agreement between the two is good, although at higher swirl ratios, radial velocities (neglected in the one-dimensional model) become more important and larger differences arise.

Figure 9 shows streamline plots, corresponding to the conditions of figure 8, included to show the formation, shape and magnitude of the recirculation bubble. For the lowest swirl, $\Omega_0 = 0.56$, the flow is nearly columnar with no reversed flow. At $\Omega_0 = 0.67$, a recirculation bubble has formed. As the swirl is further increased to $\Omega_0 = 0.78$, the front stagnation point moves upstream while the recirculation bubble grows in size. Comparison with the core area computations in figure 8 shows, as expected, that the largest differences occur in the recirculation region (which violates the assumptions in the one-dimensional model).

5.2.2. *Parametric trends for core area behaviour*

Although the axial velocity ratio is often used to characterize vortex cores, the parametric investigations we have conducted imply it is more useful to characterize the core in terms of the stagnation pressure defect relative to the free stream, i.e. in terms of the parameter, $C_{H\,\mathrm{core}}$ defined as

$$C_{H\,\mathrm{core}} \equiv \frac{\bar{H}_{\mathrm{core}} - \bar{H}_{\mathrm{outer}}}{\frac{1}{2}\rho(v_{\mathrm{max}0}^2 + W_0^2)} = \frac{1}{\Omega_0^2 + \alpha_0^2} - 1.$$

For $C_{H\,\mathrm{core}} < 0$, the core has a stagnation pressure deficit relative to the free stream. The stagnation pressure is not only a quantity of primary interest in systems such as those

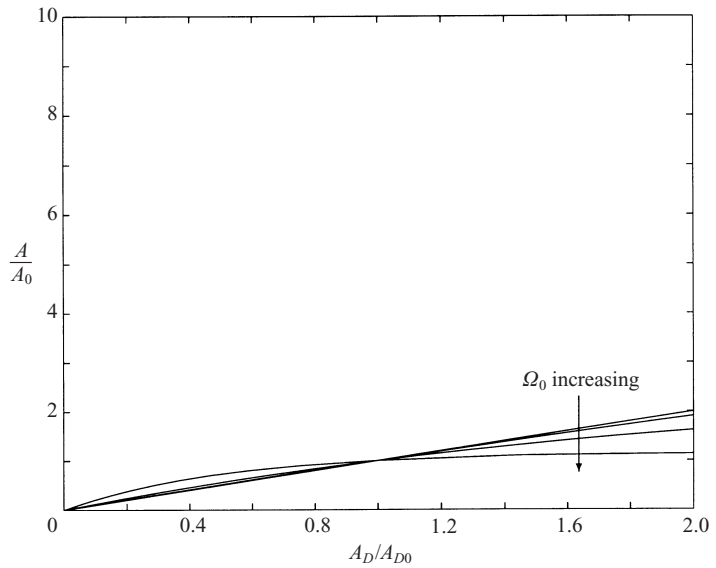

FIGURE 10. Dependence of core area, A/A_0, on duct area, A_D/A_{D0} for $C_{H\,\mathrm{core}} = 0$, $\sigma_0 = 0.01$ and $\Omega_0 = 0$, 0.3, 0.6 and 0.9. For each Ω_0, $\alpha_0 = 1.00$, 0.95, 0.80 and 0.44 respectively (α_0 becomes imaginary for $\Omega_0 \geqslant 1.0$).

related to propulsion, but, as described below, allows one to categorize the overall parametric dependence more effectively than the inlet velocity ratio, $\alpha_0 = W_0/w_0$. (Note that the claim is not that the number of parameters needed to describe the phenomenon is reduced, it is rather a question of whether one can use this reduction as a useful approximation to the overall behaviour and, if so, what set of non-dimensional parameters is most appropriate to achieve this.) For a given inlet area ratio, $\sigma_0 = A_0/A_{D0}$, it will be seen that this characterization allows a representation of core area versus duct area which approximately collapses to a limiting envelope of A/A_0 versus A_D/A_{D0}, irrespective of swirl velocity from zero to above critical. The duct area ratio at which the area increases rapidly does depend on the value of swirl at intermediate values of $C_{H\,\mathrm{core}}$, but the spread for values of Ω_0 from 0 to 1.5 is less than 25% ($C_{H\,\mathrm{core}}$ typically varies between 0 and -1.0 for practical devices; $C_{H\,\mathrm{core}} = -0.6$ is shown below to represent moderate stagnation pressure losses). In summary, casting the description in terms of flux-averaged stagnation pressure defect allows one to view some aspects of vortex core growth as roughly a function of a single parameter.

The behaviour of the core area ratio, A/A_0, is now examined as different parameters, $C_{H\,\mathrm{core}}$, σ_0, and Ω_0, are varied. The trends illustrated are: (i) the small increase in core area that occurs with vortex cores having low stagnation pressure defect irrespective of swirl, at least up to the critical value (figure 10), (ii) the large increase in area that occurs with vortex cores having an appreciable stagnation pressure defect, again essentially irrespective of swirl (figure 11).

For moderate values of stagnation pressure defect (figure 11), the curves for higher initial swirl levels show double-valued behaviour with a maximum value of A_D/A_{D0}. Since a given curve can be thought of as the solution trajectory for a vortex core (because the flux-averaged stagnation pressure is invariant), this implies that continuous behaviour is not possible for duct area ratios larger than these

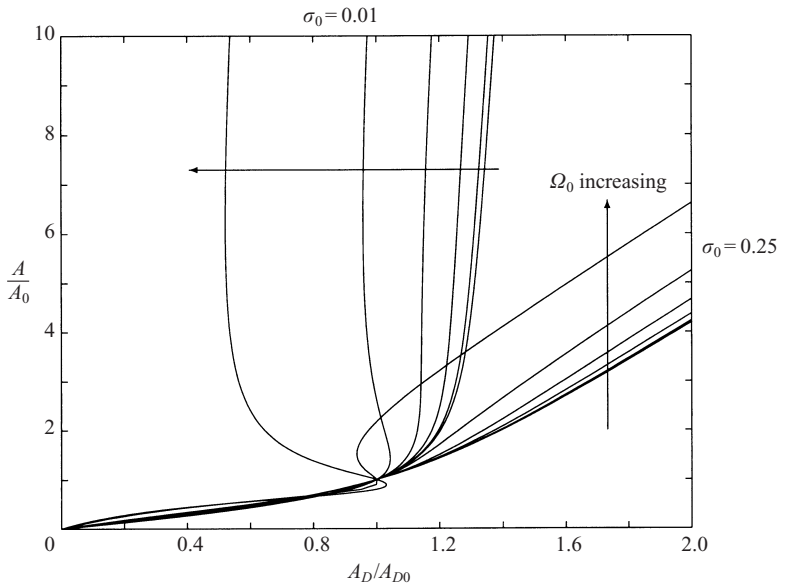

FIGURE 11. Dependence of core area, A/A_0, on duct area, A_D/A_{D0} for $C_{H\,\mathrm{core}} = -0.6$ and $\Omega_0 = 0$, 0.3, 0.6, 0.9, 1.2 and 1.5. Two inlet core-to-duct area ratios are shown, $\sigma_0 = 0.01$ and 0.25. For each Ω_0, $\alpha_0 = 1.58$, 1.55, 1.46, 1.30, 1.02 and 0.50 respectively.

maximum values. Presumably the area would jump discontinuously to a large value at a lower stagnation pressure. In the next section, we discuss the construction of such discontinuous solutions and develop an analogy with one-dimensional compressible flow and normal shock theory.

Figure 11 also depicts the strong interaction between the core and the outer flow shown by the effect of the inlet area ratio, σ_0 (core area/duct area). For the same variation in duct area ratio, cores with the higher inlet area ratio ($\sigma_0 = 0.25$) have smaller expansion, because of the decrease in outer flow area, increase in outer flow axial velocity, and thus decrease in static pressure.

6. Behaviour of steady, discontinuous vortex flows

For a stationary discontinuity there are two relations that must be satisfied by the initial and final states. We denote the left and right state by the subscripts l and r, respectively, and re-define the jump brackets as $[[f]] = f_r - f_l$. In this paper, we examine discontinuous solutions for unconfined flows only. Jump conditions and steady, discontinuous solutions can also be constructed for confined flows (Khan 1995), but the studies carried out show that, at least for the conditions investigated, the discontinuities are weak and the continuous solution appears to be a useful approximation for confined flow geometries.

In the vortex core, conservation of mass across the jump is written

$$[[Aw]] = 0. \tag{6.1}$$

Conservation of momentum is written

$$\left[\left[Aw^2 + \frac{1}{\rho}p_\delta A + \frac{\Gamma_\infty^2}{8\pi}\log A\right]\right] - \left(\frac{1}{\rho}p_{\delta_l} + \frac{\Gamma_\infty^2}{8\pi A_l}\right)[[A]] = 0. \tag{6.2}$$

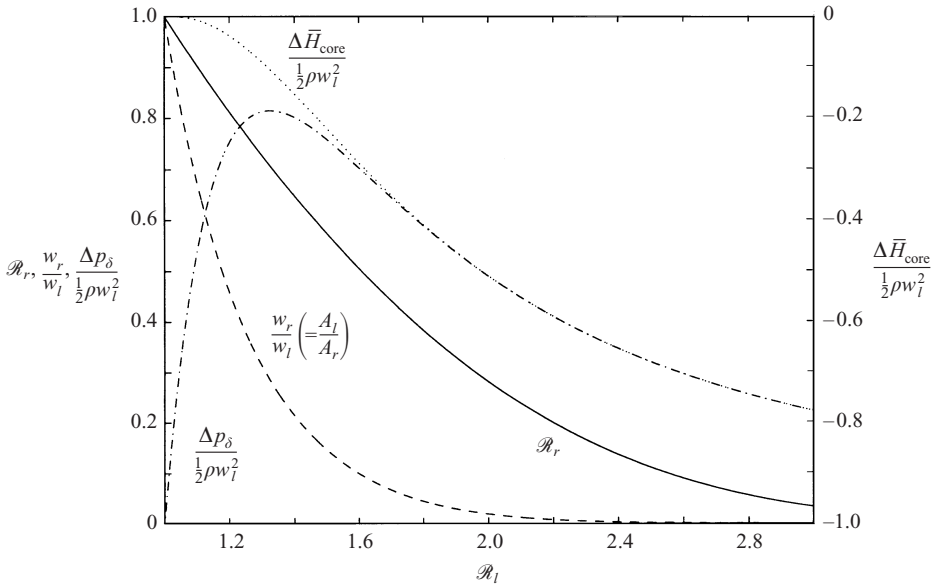

FIGURE 12. Steady shock relations: $\mathscr{R}_r$, w_r/w_l, $\Delta p_\delta/(\frac{1}{2}\rho w_l^2)$, and $\Delta \bar{H}_{\text{core}}/(\frac{1}{2}\rho w_l^2)$ versus $\mathscr{R}_l$.

We can substitute (3.5) into (6.2) and obtain an implicit relationship for the right (downstream) value of $\mathscr{R}$ in terms of the left (upstream) value of $\mathscr{R}$ (Barcilon 1967; Landahl & Widnall 1971; Lundgren & Ashurt 1989; Marshall 1991):

$$\mathscr{R}_l^2 = \frac{2\log(\mathscr{R}_r/\mathscr{R}_l)}{(\mathscr{R}_r/\mathscr{R}_l)^2 - 1}. \tag{6.3}$$

Although (6.3) admits 'shocks' which increase as well as decrease the local $\mathscr{R}$, only the latter are admissible; as shown by Marshall (1991), energy dissipation occurs across an admissible vortex shock such that the second law is satisfied. Equivalently, the flux of stagnation pressure in the core must decrease through a jump. From (5.4) and (6.3), the jump in $\bar{H}_{\text{core}}$ across a steady shock can be expressed in terms of the ratio, $\mathscr{R}_r/\mathscr{R}_l$, as

$$\frac{\Delta \bar{H}_{\text{core}}}{\frac{1}{2}\rho w_l^2} \equiv \frac{[[\bar{H}_{\text{core}}]]}{\frac{1}{2}\rho w_l^2} = \frac{2}{\mathscr{R}_l^2}\left\{\log\frac{\mathscr{R}_r}{\mathscr{R}_l}\left[\left(\frac{\mathscr{R}_r}{\mathscr{R}_l}\right)^2 + 1\right] - \left(\frac{\mathscr{R}_r}{\mathscr{R}_l}\right)^2 + 1\right\}. \tag{6.4}$$

For small-amplitude jumps, the change in $\bar{H}_{\text{core}}$ can be written as,

$$\frac{\Delta \bar{H}_{\text{core}}}{\frac{1}{2}\rho w_l^2} \approx -\frac{32}{3}(\mathscr{R}_l - 1)^3, \tag{6.5}$$

where $|\mathscr{R}_l - 1| << 1$. The loss across a discontinuous vortex jump is third order in $(\mathscr{R}_l - 1)$, analogous to the dependence of entropy rise across a shock with upstream Mach number in a compressible flow.

Figure 12 shows four quantities, $\mathscr{R}_r$, w_r/w_l $(= A_l/A_r)$, edge pressure jump $(\Delta p_\delta/\frac{1}{2}\rho w_l^2)$, and flux-averaged stagnation pressure change across the jump $(\Delta \bar{H}_{\text{core}}/\frac{1}{2}\rho w_l^2)$, as functions of $\mathscr{R}_l$. The core edge pressure rise across a jump has a maximum at roughly $\mathscr{R}_l = 1.3$ which can be motivated by the following physical considerations. From

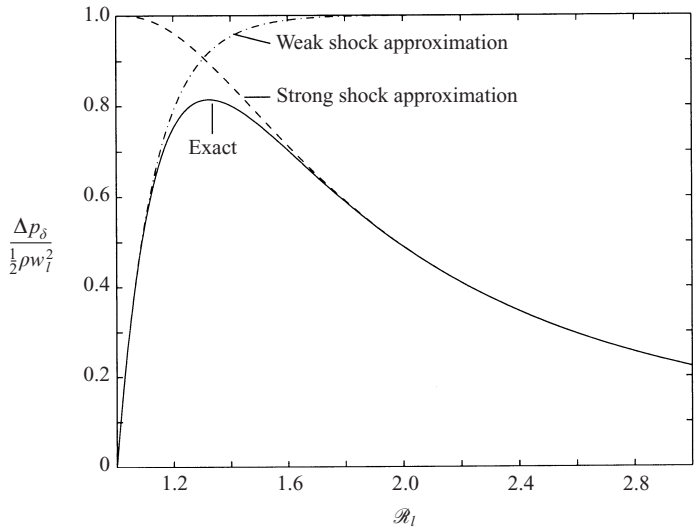

FIGURE 13. Steady shock relations. $\Delta p_\delta/(\frac{1}{2}\rho w_l^2)$, solid line. Weak shock expression (6.6), dash-dot line. Strong shock expression (6.7), dotted line.

(5.2), the pressure jump is given by

$$\Delta p_\delta = \Delta \bar{H}_{\text{core}} - \Delta(\tfrac{1}{2}\rho w^2).$$

For weak discontinuities in which the change in core stagnation pressure can be neglected (for $\mathscr{R}_l < 1.3$, $\Delta \bar{H}_{\text{core}}/\frac{1}{2}\rho w_l^2 < 0.1$), the pressure rise can be approximated as

$$\frac{\Delta p_\delta}{\frac{1}{2}\rho w_l^2} \approx 1 - \left(\frac{w_r}{w_l}\right)^2. \tag{6.6}$$

For strong discontinuities, the right state is near stagnation, so that $w_r \approx 0$ and the static pressure rise can be approximated as

$$\frac{\Delta p_\delta}{\frac{1}{2}\rho w_l^2} \approx \frac{\Delta \bar{H}_{\text{core}}}{\frac{1}{2}\rho w_l^2} + 1. \tag{6.7}$$

The validity of the latter approximation can be inferred from figure 12 in which the curves of Δp_δ and $\Delta \bar{H}_{\text{core}}$ virtually coincide for $\mathscr{R}_l$ greater than 1.7 (taking into account the different y-axis scales). The maximum core edge pressure rise is thus seen as marking the transition between nearly lossless discontinuities in which the core edge pressure rise increases with upstream $\mathscr{R}$ and highly dissipative discontinuities in which the pressure rise decreases with upstream $\mathscr{R}$. Figure 13 shows the weak and strong discontinuity approximations for the edge pressure rise, which cross at roughly $\mathscr{R} = 1.3$, compared to the exact from figure 12.

The jump conditions may also be superimposed on figure 3 as connections between supercritical and subcritical states. This is done in figure 14 which shows the admissible jump states as the end points of the dashed lines. The arrows indicate that jumps can only occur from supercritical to subcritical states. Figure 14 is the key to construction of continuous and discontinuous steady vortex flow solutions. If the flow behaves smoothly, $\mathscr{R}$ varies along the solid line in accordance with changes in the far-field pressure. At a discontinuous transition, the vortex transitions from a supercritical state to a subcritical state, which are the end points of the dashed lines in figure 14.

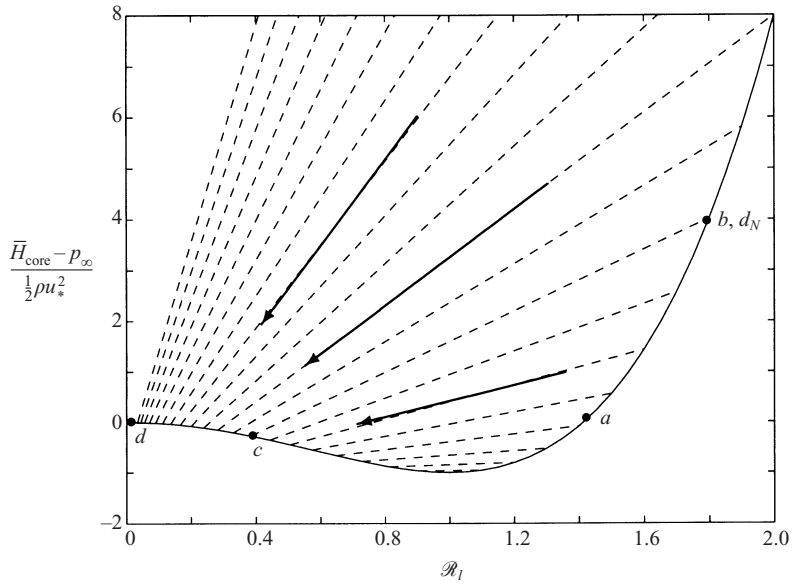

FIGURE 14. Variation with $\mathscr{R}$ of the relationship of stagnation pressure, $\bar{H}_{\text{core}}$, and far-field pressure, p_∞, for a steady flow. Admissible jump states connected by dashed line with arrows indicating that jumps can only occur from $\mathscr{R} > 1$ to $\mathscr{R} < 1$. The points a–d correspond to the solution shown in figure 15, specifically, a is the upstream state, b is the state on the upstream side of the jump, d_N is the non-dissipative downstream state, c is the state on the downstream side of the jump, and d is the downstream state.

The stagnation pressure loss across the jump is the difference in the value of the ordinate between the two states.

We can illustrate the application of figure 14 to the construction of a family of steady vortex flow solutions. In addition to the far-field pressure coefficient C_{p_∞} and the stagnation pressure coefficient C_H defined in (5.7) and (5.8), it is helpful to make use of the non-dimensional edge pressure coefficient,

$$C_p \equiv \frac{p_\delta - p_{\infty a}}{\frac{1}{2}\rho u_*^2}.$$

The non-dimensional forms of (3.5) and (5.4) are

$$C_p = C_{p_\infty} - 2\mathscr{R}^2, \tag{6.8}$$

$$C_H = C_{p_\infty} + \mathscr{R}^2(\mathscr{R}^2 - 2). \tag{6.9}$$

Consider a vortex which is initially supercritical far upstream. Because the upstream condition is supercritical, we may completely specify the upstream state, which amounts to setting the upstream $\mathscr{R}$ as $\mathscr{R}_a$. In the example, $\mathscr{R}_a = 1.414$ (i.e. $v_{\max}/w = 1$) giving $C_{Ha} = 0.0$ and $C_{p_a} = -4.0$ corresponding to point a in figure 14. This upstream level of swirl is high but not uncommon for vortices (Sarpkaya 1971).

The vortex is subjected to a far-field pressure, $C_{p_\infty}(z)$, and at a downstream location we set the edge pressure, C_{p_d}. This is analogous to a supersonic channel flow with the back pressure specified. For illustration we use a far-field pressure distribution given by

$$C_{p_\infty} = C_{p_{\infty d}} \frac{1 + \tanh z}{2},$$

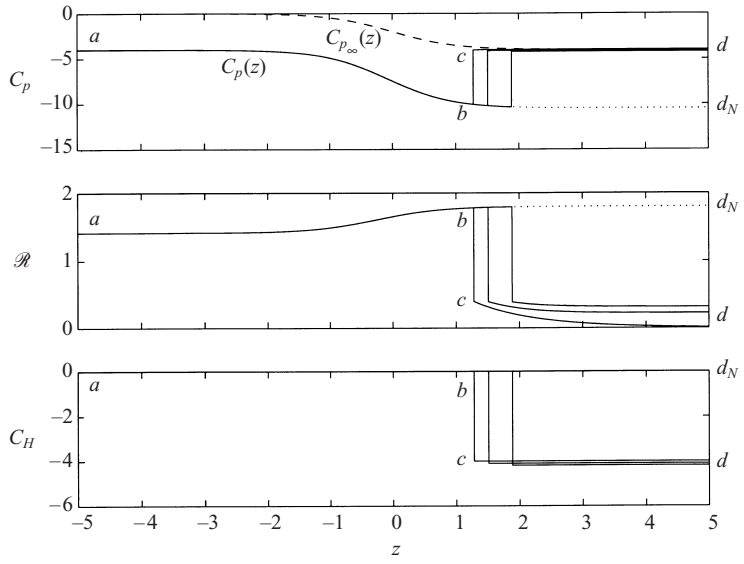

FIGURE 15. Steady vortex flow solutions. $C_{p_{\infty d}} = -4.0$, $\mathscr{R}_a = 1.414$. Dashed line, $C_{p_\infty}(z)$. Dotted line, non-dissipative (smoothly varying) solution. Downstream pressures are $C_{p_d} = -4.0$, -4.1 and -4.2.

with upstream location at $z \to -\infty$ and downstream location at $z \to +\infty$; this distribution has been previously used in numerical studies of vortical flows (Délery, Pagan & Solignac 1987) and is similar to pressure distributions measured in the delta wing experiments of Pagan & Solignac (1986). In the example, we set $C_{p_{\infty d}} = -4.0$ giving the favourable pressure gradient indicated by the dashed line in figure 15.

One possible steady solution is $C_H = C_{Ha}$ throughout the entire domain. In this case, we can solve for $\mathscr{R}(z)$ using (6.9) and the given far-field pressure. In figure 14, the location of the downstream state for constant C_H is marked by d_N, and a non-dissipative evolution of the vortex core occurs along the solid line from a to d_N. The variation of C_p and $\mathscr{R}$ versus axial location for this situation is shown in figure 15 as the dotted line with end points a and d_N.

If the downstream edge pressure is greater than the downstream edge pressure for the non-dissipative solution, vortex 'shocks' are needed to match the downstream edge pressure conditions. In the case shown, the initially supercritical flow varies smoothly along the solid line from the upstream condition at point a to point b. At point b, the vortex core undergoes a discontinuous jump to the subcritical state at point c. From point c, the flow again varies smoothly to the exit at point d.

For the conditions given, vortex shocks exist in the domain $-4.3 < C_{p_d} < -4.0$. Figure 15 shows the C_p, $\mathscr{R}$, and C_H values for three downstream edge pressures between these limits, $C_{p_d} = -4.0$, -4.1, and -4.2 (the $C_{p_d} = -4.3$ case is not shown since the jump occurs exactly at the exit). The flow states on the upstream and downstream side of the jumps are at points b and c, respectively which are also labelled in figure 14. For the conditions chosen, the upstream jump state, b, and the non-dissipative discharge state, d_N, are nearly identical.

Although the existence of vortex shocks as models for vortex breakdown and the analogy of vortex breakdown to compressible flows are appealing, care must be taken in the interpretation. In particular, vortex breakdown typically occurs over several core radii rather than over very short distances as in compressible flow shocks. In

accord with comments made previously, the analysis is then strictly valid only for vortex breakdowns that occur over distances short relative to other length scales (i.e. the length of the axial pressure variation for unconfined flows or the duct length for confined flows). While the quasi-one-dimensional model has been shown to provide good qualitative and, in many cases, quantitative predictions of vortex development prior to the occurrence of breakdown (including the onset of breakdown), a need exists to better understand the appropriate interpretation of the vortex shock solutions (i.e. core size jump, stagnation pressure loss, location of steady shocks, etc). However, currently available experimental data do not readily facilitate this investigation.

7. Conclusions

A quasi-one-dimensional description of swirling vortex core flows has been developed to characterize the overall behaviour of such fluid motions, in confined and unconfined geometries and over a range of flow regimes. The analysis, which has direct analogues with one-dimensional compressible flow and shallow-water wave phenomena, allows one to illustrate, in a simple manner (i) wave propagation on vortex cores including Kelvin–Helmholtz instability resulting from the difference of the core and outer flow axial velocity and the stabilizing effect of swirl, (ii) the classification of flow regimes depending on the ability of such waves to travel only downstream (supercritical) or both upstream and downstream (subcritical), and (iii) evolution of the vortex core area in response to external conditions including identification of those situations in which large expansions of the core area are to be expected. These last occur at the location at which the core is locally critical with respect to wave propagation. For unconfined flows, the analysis leads to the simple result that the core criticality occurs when the swirl ratio is less $\sqrt{2}$, with a similar, but algebraically somewhat more complicated expansion for confined flows.

For unconfined vortices, the analysis shows that a maximum far-field pressure rise exists above which no steady, continuous solutions are possible and that the vortex is locally critical at this maximum pressure rise. Discontinuous solutions, analogous to shocks in quasi-one-dimensional compressible flow, are therefore constructed. For one specific downstream core pressure, the flow varies smoothly; any higher back pressures result in the formation of a discontinuous jump in core properties. For a confined flow the analysis shows, in a similar fashion, that there is a maximum duct area ratio above which no steady continuous solutions are possible. This again occurs when the vortex is locally critical. For both unconfined and confined flows, the analysis also gives information concerning ways to parameterize the conditions for which a rapid increase in the core size (such as would be seen in vortex breakdown) will occur. It is found that the flux-averaged stagnation pressure, which is an invariant for a given flow, is a useful approximate indicator for correlating the onset of vortex breakdown, with the inlet swirl ratio playing a weaker role.

To assess the applicability of the one-dimensional results comparisons have been carried out with numerical simulations of the axisymmetric Navier–Stokes equations and with experimental data. The model is found to be in good quantitative agreement with both for cases in which rapid expansion does not occur. Even for cases in which the numerical results show vortex breakdown, however, the quasi-one-dimensional approach is found to capture trends such as the local conditions at which onset of rapid core expansion occur and the overall variation in core area with initial swirl, axial velocity ratio, core/duct area ratio, and duct geometry.

The authors would like to acknowledge the H. N. Slater Professorship for facilitating the collaboration between individuals originally at three different institutions. We would also like to thank Dr J. Délery for providing information concerning experiments on vortex breakdown. D. L. Darmofal would like to acknowledge the kind support of the Departments of Aerospace Engineering at the University of Michigan and Texas A&M University where a portion of this work was performed.

REFERENCES

Barcilon, A. 1967 Vortex decay above a stationary boundary. *J. Fluid Mech.* **27**, 155–175.

Batchelor, G. K. 1964 Axial flow in trailing line vortices. *J. Fluid Mech.* **20**, 645–658.

Benjamin, T. B. 1962 Theory of the vortex breakdown phenomenon. *J. Fluid Mech.* **14**, 593–629.

Beran, P. S. & Culick, F. E. C. 1992 The role of nonuniqueness in the development of vortex breakdown in tubes. *J. Fluid Mech.* **242**, 491–528.

Cho, D. 1995 Effect of vortex core stagnation pressure on tip clearance flow blockage in turbomachines. Master's thesis, MIT.

Darmofal, D. L. 1993 A study of the mechanisms of axisymmetric vortex breakdown. PhD thesis, MIT.

Darmofal, D. L. 1996 Comparisons of experimental and numerical results for axisymmetric vortex breakdown in pipes. *Computers Fluids* **25**, 353–371.

Darmofal, D. L. & Murman, E. M. 1994 On the trapped wave nature of axisymmetric vortex breakdown. *AIAA Paper* 94-2318.

Délery, J., Pagan, D. & Solignac, J. 1987 On the breakdown of a vortex induced by a delta wing. In *Vortex Control and Breakdown Behavior Conference*. Baden.

Drazin, P. G. & Reid, W. H. 1981 *Hydrodynamic Stability*. Cambridge University Press.

Faler, J. H. & Leibovich, S. 1977 Disrupted states of vortex flow and vortex breakdown. *Phys. Fluids* **20**, 1385–1400.

Howard, L. N. 1963 Fundamentals of the theory of rotating fluids. *J. Appl. Maths* **30**, 481–485.

Khan, R. 1995 A quasi one-dimensional analysis for confined vortex cores. Master's thesis, MIT.

Krishnamoorthy, S. & Marshall, J. S. 1994 An experimental investigation of "vortex shocks". *Phys. Fluids* **6**, 3737–3741.

Lamb, H. 1932 *Hydrodynamics*. Cambridge University Press.

Landahl, M. T. & Widnall, S. E. 1971 Vortex control. In *Aircraft Wake Turbulence and its Detection* (ed. A. Goldburg, J. H. Olsen & M. Rogers). Plenum.

Leibovich, S. 1983 Vortex stability and breakdown: Survey and extension. *AIAA J.* **22**, 1192–1206.

Leonard, A. 1994 Nonlocal theory of area-varying waves on axisymmetric vortex tubes. *Phys. Fluids* **6**, 765–777.

Lundgren, T. S. & Ashurst, W. T. 1989 Area-varying waves on curved vortex tubes with application to vortex breakdown. *J. Fluid Mech.* **200**, 283–307.

Mahesh, K. 1996 A model for the onset of breakdown in an axisymmetric compressible vortex. *Phys. Fluids* **8**, 3338–3345.

Marshall, J. S. 1991 A general theory of curved vortices with circular cross-section and variable core area. *J. Fluid Mech.* **229**, 311–338.

Marshall, J. S. 1993 The effect of axial pressure gradient on axisymmetrical and helical vortex waves. *Phys. Fluids* A **5**, 588–599.

Marshall, J. S. & Krishnamoorthy, S. 1997 On the instantaneous cutting of a columnar vortex with non-zero axial flow. *J. Fluid Mech.* **351**, 41–74.

Pagan, D. 1989 Contribution à l'étude expérimentale et théorique de l'éclatement tourbillonnaire en air incompressible. PhD thesis, Université Pierre et Marie Curie, Paris; see also *ONERA Note Technique No.* 1990-12.

Pagan, D. & Solignac, J. L. 1986 Experimental study of the breakdown of a vortex generated by a delta wing. *La Recherche Aerospatiale*, 1986-3.

Sarpkaya, T. 1971 On stationary and travelling vortex breakdowns. *J. Fluid Mech.* **45**, 545–559.

Spall, R. E., Gatski, T. B. & Grosch, C. E. 1987 A criterion for vortex breakdown. *Phys. Fluids* **30**, 3434–3440.

Yih, C. 1980 *Stratified Flows*. Academic.